PHYS4070 Assignment 3

Ryan White

24th of May, 2024

Part I: Bright Solitons in the Non-Linear Schrödinger Equation

Quantum systems describe the behaviour of (often interacting) waves on a fundamental level, requiring the solving of complex partial differential equations. The non-linear Schrödinger equation encodes the time and spatial evolution of these interacting, complex wavefunctions. The partial differential equation is given as

$$i\frac{\partial\psi}{\partial t} = -\frac{\partial^2\psi}{\partial x^2} + g|\psi|^2\psi \tag{1}$$

where the parameter g describes the self-interaction strength of the wavefunction. Starting with an initial state of the wavefunction, the state at some future time can be estimated with numerical integration schemes. Since the wavefunction is usually changing in time, we also need to use numerical differentiation methods to determine the second derivative term where an analytic second derivative isn't always possible to determine. In practice, given that we know the initial state of the wavefunction $\psi(x, 0)$, we can numerically estimate the second derivative with a second order central difference method:

$$f''(x) \approx \frac{f(x+\Delta x) - 2f(x) + f(x-\Delta x)}{(\Delta x)^2} \tag{2}$$

This is tractable across an entire domain when using fixed boundary conditions, i.e. $\psi(-X, t) = a$, $\psi(X, t) = b$, so that we can calculate the numerical second derivative at all values except the unchanging boundary (where there is no derivative, and $\partial^2\psi/\partial x^2 = 0$). For our purposes, we set $a = b = 0$, and $X = L/2 = 10$ (i.e. $L = 20$).

To evolve the system in time, we employ the Runge-Kutta 4th order (RK4) numerical integrator. The RK4 method works essentially the same as an Euler integrator, where a parameter on the next time step is equal to its current value, plus the timestep times its derivative:

$$x_{i+1} = x_i + \frac{dx_i}{dt}\Delta t \tag{3}$$

The strength in the RK4 method arises from using this method iteratively for values between 0 and Δt,

$$\mathbf{k}_1 = \mathbf{f}\left(\mathbf{X}_i,\ t_i\right) \tag{4}$$

$$\mathbf{k}_2 = \mathbf{f}\left(\mathbf{X}_i + \frac{\mathbf{k}_1\Delta t}{2},\ t_i + \frac{\Delta t}{2}\right) \tag{5}$$

$$\mathbf{k}_3 = \mathbf{f}\left(\mathbf{X}_i + \frac{\mathbf{k}_2\Delta t}{2},\ t_i + \frac{\Delta t}{2}\right) \tag{6}$$

$$\mathbf{k}_4 = \mathbf{f}\left(\mathbf{X}_i + \mathbf{k}_3\Delta t,\ t_i + \Delta t\right) \tag{7}$$

$$\mathbf{X}_{i+1} = \mathbf{X}_i + \frac{1}{6}\left(\mathbf{k}_1 + 2\mathbf{k}_2 + 2\mathbf{k}_3 + \mathbf{k}_4\right)\Delta t \tag{8}$$

Here, $\mathbf{X}_i$ is the vector of parameters (and $\mathbf{f}(\mathbf{X}_i, t_i)$ is the derivative function). Since we're only evolving the wavefunction in one dimension, this is a single element complex-valued vector with $\mathbf{X}_i = \psi_i$ (where ψ_i is the value at a given timestep), and the derivative function is

$$f(x,t) = \frac{\partial\psi}{\partial t} = i\frac{\partial^2\psi}{\partial x^2} - ig|\psi|^2\psi \tag{9}$$

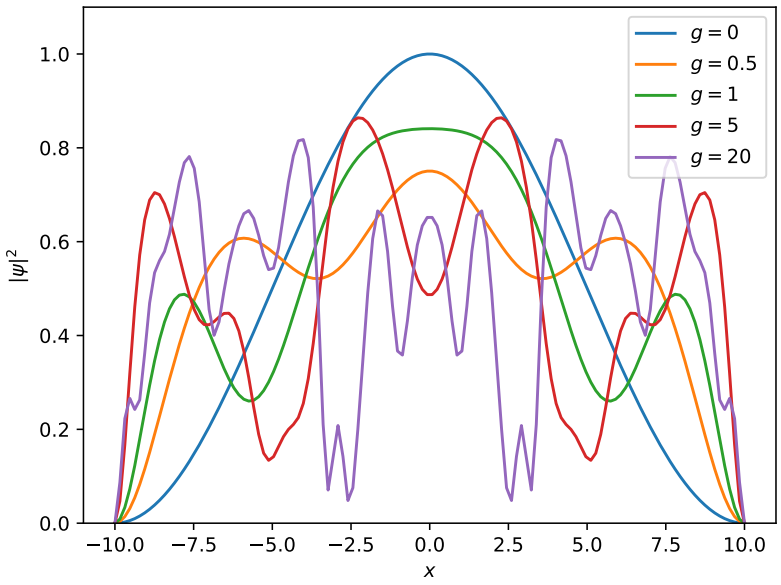

Figure. 1 A snapshot of plane wave evolution (at roughly $t \sim 15$) shows that the state has a sensitive dependency on the interaction strength, g.

As a first test of our integration scheme, we initialised a plane wave wavefunction on the interval $[-L/2,\ L/2] = [-10,\ 10]$ with the equation

$$\psi(x,\ 0) = \cos(\pi x/L) \tag{10}$$

for $N = 128$ spatial intervals. We then let this wavefunction evolve up to a time $t = 30$ in timesteps of $\Delta t = 0.01$. We show a snapshot of this evolution for several simulation runs of varying interaction strength in Figure 1, and have included an animated gif `Part1b_Plane_Wave_Evolution.gif` with the submission of this report and code. We see generally faster evolution of the wavefunction and more modes with higher interaction strength. This is to be expected due to the interaction term in Equation 1 – if $|g|$ gets larger the magnitude of the time derivative gets proportionally larger. Physically, a more positive value of g correlates to a more repulsive self-interaction in the wavefunction, and hence we would expect more modes with a faster evolution.

For the remainder of this section of the project, we set $g = -1$ in Equation 1, corresponding to an attractive self-interaction. We next model the so called 'bright soliton' wavepacket,

$$\psi(x,\ 0) = \sqrt{2}\exp(iux)\,\mathrm{sech}(x) \tag{11}$$

where we show a representative snapshot of this wavefunction in Figure 2. With this figure, and the associated animated gif `Part1c_Soliton_Evolution.gif`, we interpret the parameter u as the velocity of the soliton. The sign of u hence determines the initial direction of the soliton movement before eventually 'bouncing' off of the domain boundaries and reversing its direction of motion. Hence, $u = 0$ corresponds to a static soliton (given by the green line), $u > 0$ corresponds to initial motion in the $+x$ direction and $u < 0$ initial motion in the $-x$ direction.

We plot the peak positions of the soliton (across several runs) in the right side of Figure 2. This shows this directional initial movement of the solitons where the red and purple lines (corresponding to $u > 0$) move to positive x initially, the opposite for the blue and yellow lines ($u < 0$) and no change for the green line ($u = 0$). Two particularly interesting phenomena can be seen in this right side plot. The first of which is that the peak positions aren't exactly $u \times L/2$ periodic and oscillate at a slightly shorter period. Viewing the accompanying gif shows that the peaks don't perfectly 'bounce' off of the boundaries at $\pm L/2$, and so they can reverse their trajectory in slightly less time. Secondly, the larger $|u|$ soliton simulations exhibit sharper peak trajectories with peak positions that reach closer to the boundaries. The sort of gradual reflection points seen in the oscillatory behaviour are a result of these solitons not quite bouncing off of the exact boundary edge, where the higher velocity solitons have correspondingly more momentum to reach closer to the boundary before being bounced back.

After investigating the motion of a single soliton, the logical next step is to initialise a state with two solitons and observe the dynamics. With that in mind, we evolved two solitons initially separated by $L/2$, with velocity

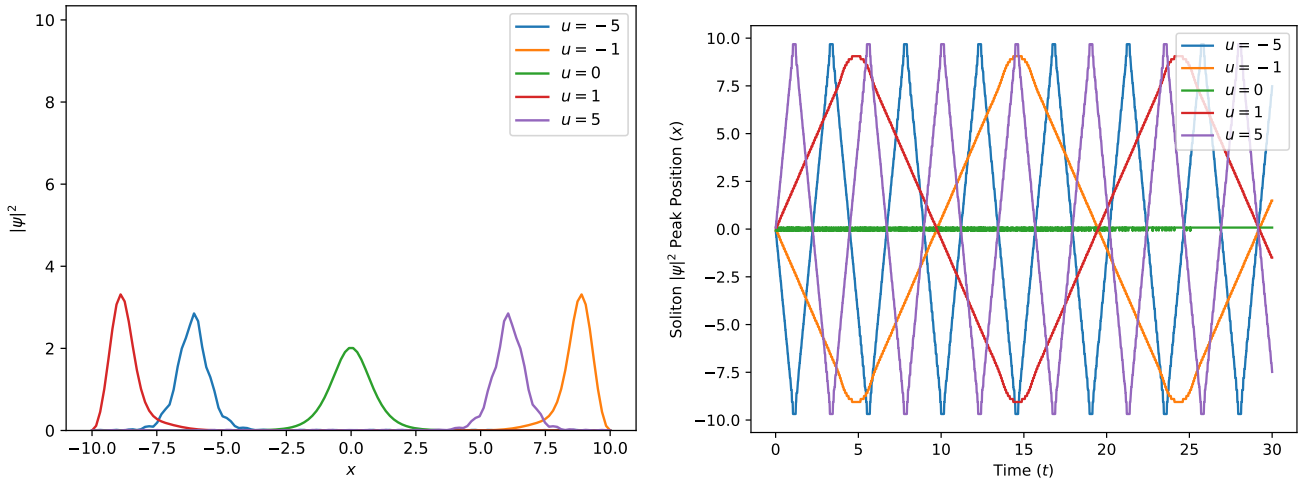

Figure. 2 *Left:* A snapshot (at $t \sim 15$) of many simulations, each of a single bright soliton, with different velocities u. We see that the magnitude of this velocity affects its periodic behaviour and direction, where the sign of u effectively determines the initial direction the soliton travels to. *Right:* We plot the x position of the soliton peaks as a function of time. As before, the velocity u of the soliton determines the speed of its evolution, and the sign determines its initial direction such that opposite signs correspond to a half-period shift in behaviour (or a mirrored image about the y-axis [$x = 0$]).

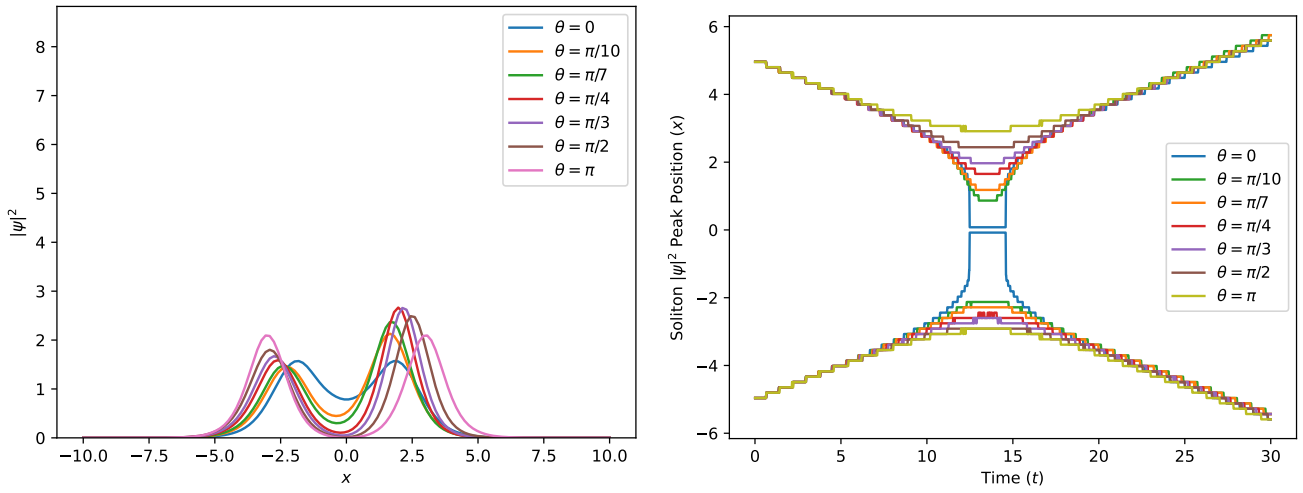

Figure. 3 *Left:* A snapshot (at $t \sim 15$) of several two-soliton simulations, each with $u = 0.1$ and varying relative phase θ. The state of the system is especially sensitive to the relative phase when the solitons are close to $x = 0$ as in this snapshot. *Right:* We plot the position of each soliton peak (assuming a bounce condition) over time. Given that all simulation runs have the same velocity u, we see the close approach of the peaks at the same time – this is an indication that the close approach distance is a function of phase.

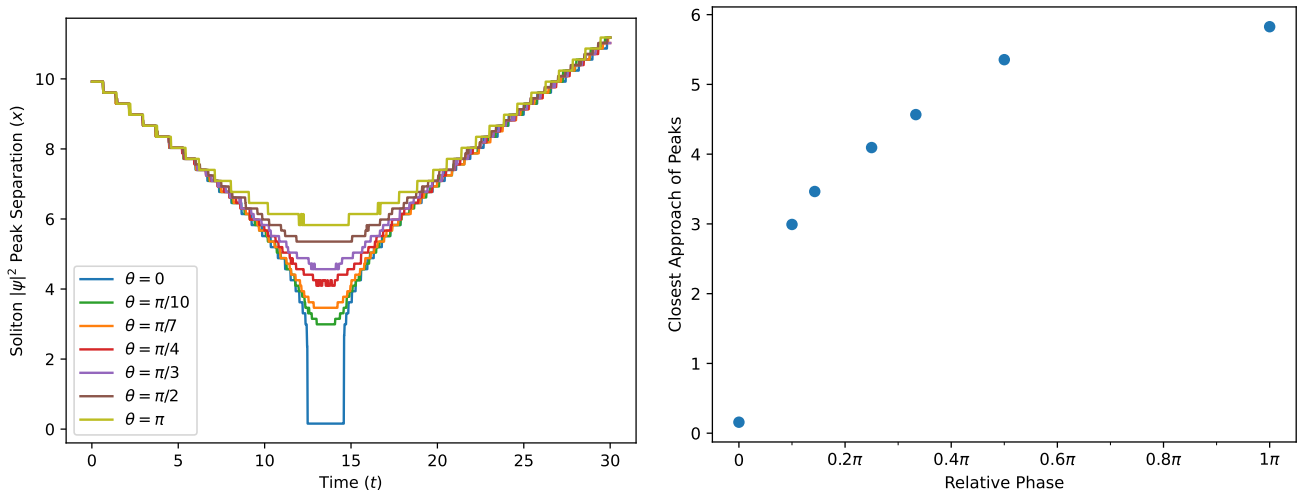

Figure. 4 *Left:* We plot the separation between the two soliton peaks as a function of time, using the same data as in Figure 3. *Right:* The minimum separation, or closest approach, of the two peaks as a function of relative phase can be taken from the left plot. Since the relative phase is 2π periodic, we'd expect the close approach behaviour for $\theta \in [\pi,\ 2\pi]$ to be the mirrored image (about the y-axis) of that for $\theta \in [0,\ \pi]$ (i.e. it would begin to decrease again for values to the right of our plotted domain).

$u = 0.1$ and a variable relative phase parameter θ:

$$\psi(x,\ 0) = \sqrt{2}\exp(iux)\,\mathrm{sech}(x + L/4) + \sqrt{2}\exp(-iux + i\theta)\,\mathrm{sech}(x - L/4) \tag{12}$$

We see here that the left soliton (with $x + L/4$ in the sech term) has a positive velocity and hence moves to the right, while the right soliton (the right term) has a negative velocity. The result is some 'collision' between the solitons at $x = 0$ after some time (specifically about $t \sim 13$ in our simulation). A snapshot just after this collision/merger/bounce is shown in Figure 3 and `Part1d_Solitons_Evolution.gif` shows the evolution as an animated gif.

Since each of our component solitons move independently of each other, as they pass over each other (or bounce) around $x = 0$ the wave packets could constructively/destructively interfere with each other to produce the observed $|\psi|^2$ distribution. Given that the solitons are potentially out of phase with each other by θ, we get destructive behaviour right at $x = 0$ as a function of θ – we get complete destructive interference for $\theta = \pi$, and complete constructive interference for $\theta \in \{0,\ 2\pi\}$. Considering the norm-squared of the superposition of these two solitons, we obtain

$$|\psi_1 + \psi_2|^2 = |\psi_1|^2 + \psi_1^*\psi_2 + \psi_1\psi_2^* + |\psi_2|^2 \tag{13}$$

$$= \frac{e^{-iux}e^{-iux+i\theta} + e^{iux}e^{iux-i\theta}}{\cosh(x + L/4)\cosh(x - L/4)} + |\psi_1|^2 + |\psi_2|^2 \tag{14}$$

$$= \frac{2\cos(2ux - \theta)}{\cosh(x + L/4)\cosh(x - L/4)} + |\psi_1|^2 + |\psi_2|^2 \tag{15}$$

Hence the cosine cross term provides an extra term in the sum whose value is between ± 2 about $x = 0$ depending on the value of θ. This produces the constructive/destructive interference inherent of the interacting solitons. With more destructive interference, we'd expect that the peaks of the solitons remain independent which would correspond to a large 'close approach' distance. This is exactly what we see in the right plot of Figure 4.

Another key behaviour of the two soliton model lies in the asymmetry of the peak magnitudes about $x = 0$; when the solitons approach each other in Figure 3, the left peak has a lower magnitude than the right peak. The explanation for this lies in our treatment of the relative phase, as this is the only asymmetry in Equation 12. As we only plotted positive relative phases we see this same behaviour in each simulation run, however if we plotted negative relative phases we'd see the opposite behaviour: the left peak being characterised by a *higher* magnitude than the right when the solitons approach $x = 0$. As a consistency check, the included animation shows that a relative phase of $\theta = 0$ (i.e. the midway point between positive and negative phase) exhibits a perfectly symmetric evolution and peak as expected.

In summary, we investigated the time evolution of interacting complex waves using a `C++` implementation of the RK4 numerical integration scheme. We showed that, with strict 0 boundary conditions, that simple systems (a plane wave in our case) as well as more complex systems (solitary and interacting solitons) exhibit interesting dynamics especially for strong self-interactions. In the latter case, we showed that pairs of interacting solitons are extremely sensitive to the relative phase of the two wave packets and can produce strong constructive and destructive interference in the combined wavefunction as a result.

Part II: The Transverse Ising Spin Model

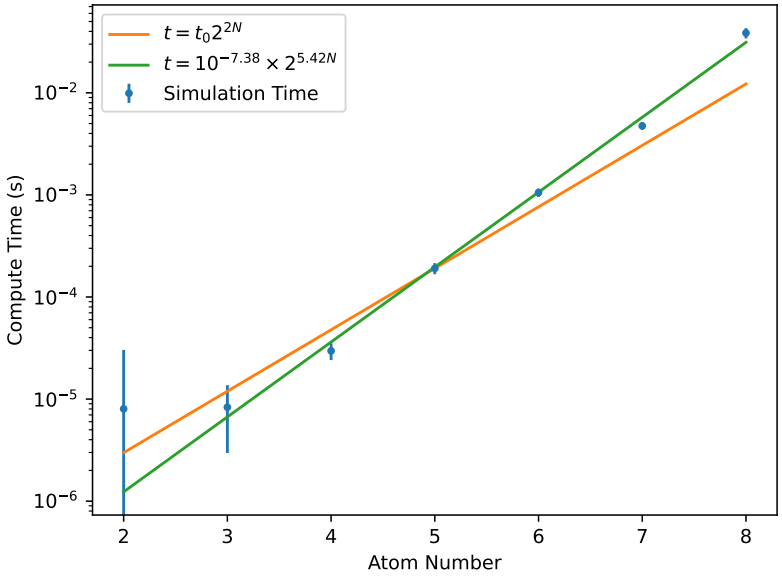

Figure. 5 We timed the process of constructing the Hamiltonian and determining its eigenvalues/vectors as a function of atom number. On a log-linear plot the code duration appears approximately linear, indicative of an exponential function. We plot here the average and standard deviation across 20 samples at each atom number. Overlaid are two lines: a $t_0 \times 2^{2N}$ trendline, where t_0 is normalised to the $N = 5$ value chosen due to the data linearity around that point, and a best fit trendline (omitting the first data point) where we see an exponential power $> 2N$.

As another example of a 'many body' quantum system, we next investigate the 1-dimensional transverse Ising spin model. This models the quantum effects of several particles interacting with each other, and exhibits much of the same behaviour as the classical thermodynamic Ising model (e.g. phase transitions, time evolution, etc). The Hamiltonian for such a many body quantum Ising system is

$$\hat{H} = -\sum_{m=0}^{N-1} \hat{\sigma}_z^{(m)} - g \sum_{m=0}^{N-1} \hat{\sigma}_x^{(m)} \hat{\sigma}_x^{(m+1)} \tag{16}$$

where N is the number of particles, g is the nearest-neighbour interaction strength (as in the first part of the project), and the Pauli spin matrices are

$$\hat{\sigma}_z^{(m)} = I^{\otimes m} \otimes \begin{pmatrix} 1/2 & 0 \\ 0 & -1/2 \end{pmatrix} \otimes I^{\otimes(N-1-m)}; \qquad \hat{\sigma}_x^{(m)} = I^{\otimes m} \otimes \begin{pmatrix} 0 & 1/2 \\ 1/2 & 0 \end{pmatrix} \otimes I^{\otimes(N-1-m)} \tag{17}$$

Here I is the 2×2 identity matrix, where the superscript $\otimes$ notation describes the repeated self-tensor product. The calculation of the right term in Equation 16 can be simplified by evaluating

$$\hat{\sigma}_x^{(m)} \hat{\sigma}_x^{(m+1)} = I^{\otimes m} \otimes \begin{pmatrix} 0 & 1/2 \\ 1/2 & 0 \end{pmatrix} \otimes \begin{pmatrix} 0 & 1/2 \\ 1/2 & 0 \end{pmatrix} \otimes I^{\otimes(N-2-m)} \tag{18}$$

as opposed to manually performing the matrix product.

To model the 1-dimensional chain, we enforce periodic boundary conditions such that the Nth spin matrix is actually the 0th spin matrix, $\hat{\sigma}_x^{(N)} = \hat{\sigma}_x^{(0)}$. Immediately we see that this changes the evaluation of the rightmost term of Equation 16 when $m = N - 1$, effectively creating a mathematical (but not physical) discontinuity in the spin matrix superscript of Equation 18. To account for this, at the $(N-1)$th summation we instead evaluate

$$\hat{\sigma}_x^{(m)}\hat{\sigma}_x^{(m+1)} = \hat{\sigma}_x^{(N-1)}\hat{\sigma}_x^{(N)} = \begin{pmatrix} 0 & 1/2 \\ 1/2 & 0 \end{pmatrix} \otimes I^{\otimes(N-2)} \otimes \begin{pmatrix} 0 & 1/2 \\ 1/2 & 0 \end{pmatrix} \tag{19}$$

instead of manually multiplying the matrices to maximise computational efficiency.

After the $2^N \times 2^N$ Hamiltonian matrix is constructed for an N-body system, we can determine the eigenvectors and eigenvalues numerically with the `LAPACK` library. Specifically, we use the `dsyev_` function to solve the $A\mathbf{u} = \lambda\mathbf{u}$ eigenvalue/vector problem. Since the Hamiltonian dimension scales exponentially with the number of spins, we would expect the compute time (of the Hamiltonian construction and eigenproblem solving) to also scale similarly. We show the compute time in Figure 5 on a log-linear plot, where we see this exact trend (a positive linear slope on a log-lin plot translates to exponential growth). We wouldn't necessarily expect that the process scales as 2^{2N} due to the fact that we also time the eigenproblem solving at the same time, adding an extra layer of complexity and making the compute time slope steeper (as we see in Figure 5).

With the code written and benchmarked, we now focus on using it to investigate the transverse Ising spin model. One interesting calculation we can focus on is the ground state energy per particle $\mathcal{E}_0/N$ of the system. This has an analytic solution in the thermodynamic limit, given by

$$\lim_{N\to\infty}\left\{\frac{\mathcal{E}_0}{N}\right\} = -\frac{(2+g)}{2\pi}\,\mathrm{E}\left[\frac{8g}{(2+g)^2}\right] \tag{20}$$

with

$$\mathrm{E}[x] \approx \frac{\pi}{2M}\sum_{k=0}^{M}\sqrt{1 - x\sin^2\left(\frac{\pi k}{2M}\right)} \tag{21}$$

We plot the results of our simulation (for $N = 8$) in comparison to this result in the thermodynamic limit in Figure 6. Immediately we see some interesting behaviour in the model. Looking at the ground state energy per spin (top panel in Figure 6), we see that the energy tends towards $\mathcal{E}_0/N = -0.5$ for $g \to 0$ and towards $\mathcal{E}_0/N \approx -g/4$ for $g \gg 2$. Further, the residuals in our numerical data compared to the analytic solution (albeit in the thermodynamic limit) have the largest magnitude centered about $g = 2$. We interpret this as a quantum phase transition in the Ising spin model centered at $g = 2$. Intuitively, the largest discrepancy in theory and observation would occur at the phase transition where the system is most sensitive to parameter changes. We note that $g = 0$ corresponds to no spin-spin interaction in the x-direction (the interaction term in the Hamiltonian, Equation 16, goes to 0) and so we would expect that all spins would be aligned anti/parallel along the z-direction in this case. I interpret this limiting ground state energy of $\mathcal{E}_0/N = -0.5$ arising from the $1/2$ terms in the z Pauli spin matrix.

As we increase the interaction term g, the particles then proceed to interact more strongly along the x direction. Hence, at $g = 2$, the most bound (negative) energy state of the system is one where the spins are aligned more along the x direction than the z direction. This produces the phase transition we observe. As we continue increasing g, the spins preference alignment in the x direction (over the z direction) more and more which produces the observed negative slope. I interpret the magnitude of this slope, $g/4$, being the result of two $1/2$ multiplications due to the nearest-neighbour interaction along each direction from the x Pauli spin matrix multiplication, Equation 18 and Equation 19.

Finally, we show the second derivative of this ground state energy per spin in the lower panel of Figure 6. The spike in the analytic second derivative (recall, at $N \to \infty$) shows that we should expect a phase transition at $g = 2$. The discrepancy between the numerical and analytic curve here is due to our simulation with $N = 8$ particles to reduce computation time, as opposed to an arbitrarily large N characteristic of the thermodynamic limit in a macroscopic system. Regardless, the ground state energy curve has an error $\lesssim 1\%$ across the entire domain which is accurate enough for our purposes.

We now turn our interest to how the $N = 8$ system evolves in time when quenched from the ground state of $g = 0$ to $g = 4$ – a sort of quantum equivalent of creating a wave in a still pool of water. To do this, we construct the Hamiltonian in a $g = 0$ state where all spins are anti/aligned along the z axis. The initial wavefunction, $\psi(0)$, is the ground state eigenvector of this. Then, we evolve the system according to

$$\psi(t) = e^{-i\hat{H}t}\psi(0) \tag{22}$$

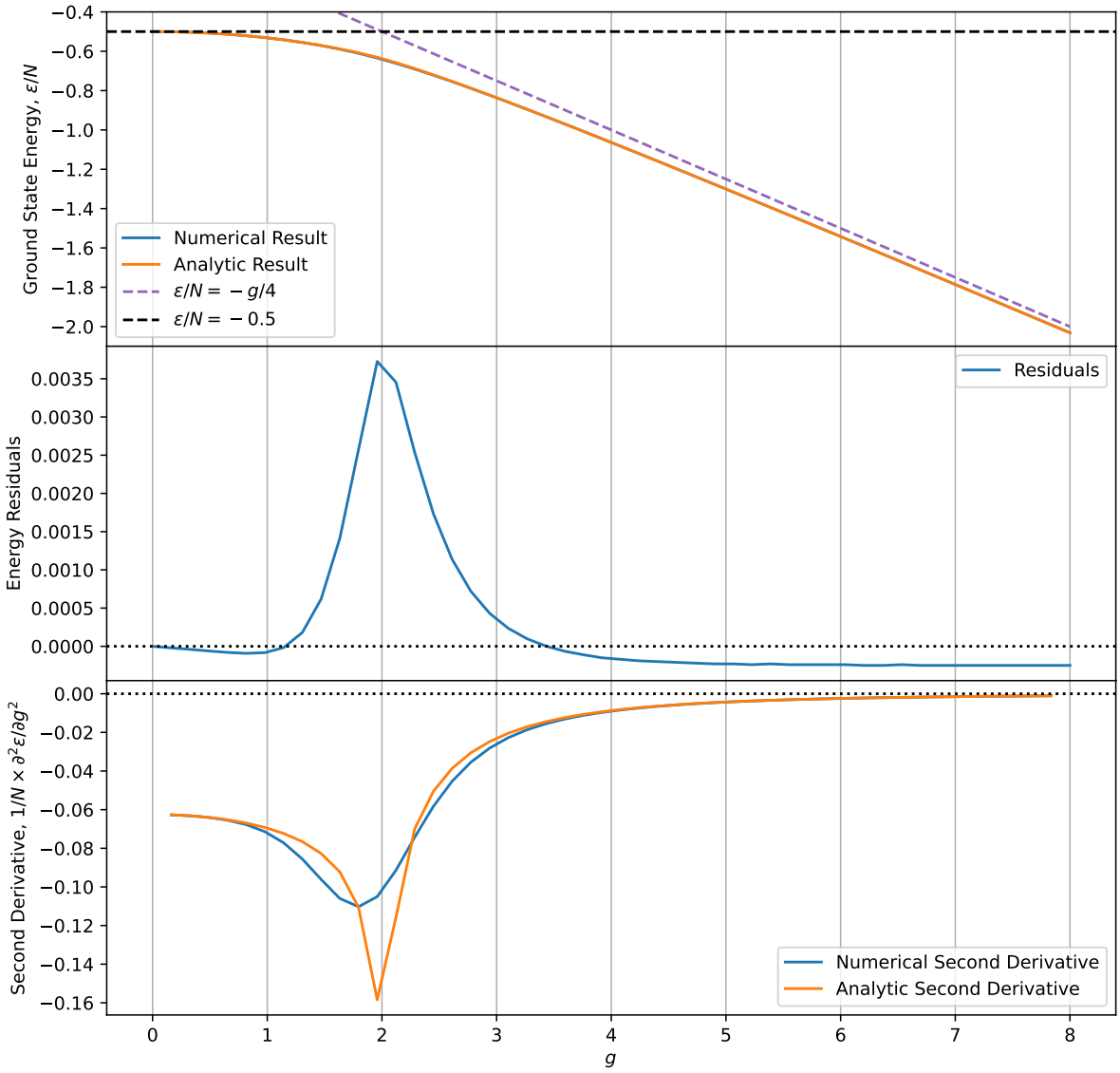

Figure. 6 We plot the ground-state energy (per spin) as a function of interaction strength, g. The analytic result in the thermodynamic limit is overlaid, calculated from Equation 20. We plot the residuals of the numerical and analytic result in the second panel, showing broad agreement for a range of g where the main discrepancy is centered around $g \sim 2$. Using the second derivative formula (Equation 2), we estimate the second derivatives of our numerical result and the analytic formula in the bottom panel, again showing discrepancy around $g \sim 2$.

where $\hat{H}$ is the Hamiltonian of the $g = 4$ system. For the purposes of solving this evolution within `C++` code, it is easier to solve the

$$\psi(t) = Ue^{-iDt}U^{\dagger}\psi(0) \tag{23}$$

problem, where U is the matrix of eigenvalues of the $g = 4$ state and D is the diagonal matrix of eigenvalues of $\hat{H}$. A further simplification can be made, noting that the state at any time $t = N\Delta t$ is the product of the state at each timestep. That is, $e^{-iDt} = (e^{-iD\Delta t})^N$. Since the eigenvectors/values are constant in time (we only change values of g initially and never again), we can evolve the system on each time step by evaluating

$$\psi(t + \Delta t) = Ue^{-iD\Delta t}U^{\dagger}\psi(t) \tag{24}$$

where $Ue^{-iD\Delta t}U^{\dagger}$ only needs to be evaluated once prior to evolving the system in time. This means that only one matrix multiplication needs to be carried out on each timestep, rather than four.

As a measure of how the system is changing over time, in Figure 7 we plot the observables S_z, S_x, and C_{xx}, which are calculated by

$$S_z = \sum_{m=0}^{N-1} \langle \hat{\sigma}_z^{(m)} \rangle \tag{25}$$

$$S_x = \sum_{m=0}^{N-1} \langle \hat{\sigma}_x^{(m)} \rangle \tag{26}$$

$$C_{xx} = \sum_{m=0}^{N-1} \sum_{\substack{n=0 \\ n \neq m}}^{N-1} \langle \hat{\sigma}_x^{(m)} \hat{\sigma}_x^{(n)} \rangle \tag{27}$$

Here S_z is the expectation of the z spin alignment and S_x is analogous for the x direction. As an example, we calculate S_z as

$$S_z = \langle \psi(t) | \sum_{m=0}^{N-1} \hat{\sigma}_z^{(m)} \ | \psi(t) \rangle \tag{28}$$

where $\hat{\sigma}_z^{(m)}$ is the Pauli z matrix as in Equation 17, and this calculation is analogous for the other observables. Calculating this on each step we see the time evolution in Figure 7.

We test this time evolution for values of $g = \{1, 4, 20\}$; immediately we see a quasi-periodic behaviour in the S_z and C_{xx} observables. Beginning from $S_z = 4$ and $C_{xx} = 0$ (characteristic of the $g = 0$ ground state), an oscillating behaviour of period $P \sim \{10, 5, 4\}$ time units (for each increasing g value) begins. Since the system was initialised with $g = 0$ for each run, there was no initial spin alignment along the x axis as the x interaction term was 0. This behaviour was 'frozen in' to the system such that even after quenching, there remains no net spin along the x direction. This doesn't necessarily mean that there is no local spin along the x direction, however, and the C_{xx} term encodes at least *some* of the information about correlations of x direction spin between neighbouring pairs of particles. This means that we can in principle get some localised spin alignment along the x direction which also means that we would expect correspondingly less net spin along the z direction. In fact, we see exactly this in Figure 7 where peaks of S_z correspond to troughs of C_{xx} and vice versa. We can then interpret the oscillatory behaviour of the system as kind of 'density waves' of spin flipping moving through the system.

Further, we can see that for values of $g > 1$ the observable S_z oscillates about 2. We posit that this corresponds to roughly equal spins along each of the x and z directions (on average over time) after the phase transition at $g = 2$. As before, we expect no net spin along the x direction, but perhaps regions of very correlated spins that cancel out overall. In the $g = 1$ case, we instead see quasi-periodicity about $S_z \sim 3.5$, where the interaction term between particles isn't quite strong enough to enforce equal spins along the z and x directions (i.e. there is always more localised spin along z than x for nearest neighbours). Finally, for the highest g values we see the sharpest variability in the observables. We interpret this as the strong spin-spin interaction violently flipping nearest neighbours and overextending past the equilibrium, therefore flipping back after some time.

To summarise, we created a `C++` implementation of the transverse Ising spin model, using it to investigate the behaviour of a many body quantum system. We showed that the model exhibits a phase transition in the spin alignment at $g = 2$ and that a quenched system is characterised by complex but quasi-periodic behaviour. In the latter case, we noticed that behaviour intrinsic to the initial state can be frozen in to the system such that some aspects of its evolution are limited (in this case, no net spin along the x direction is observed for any time).

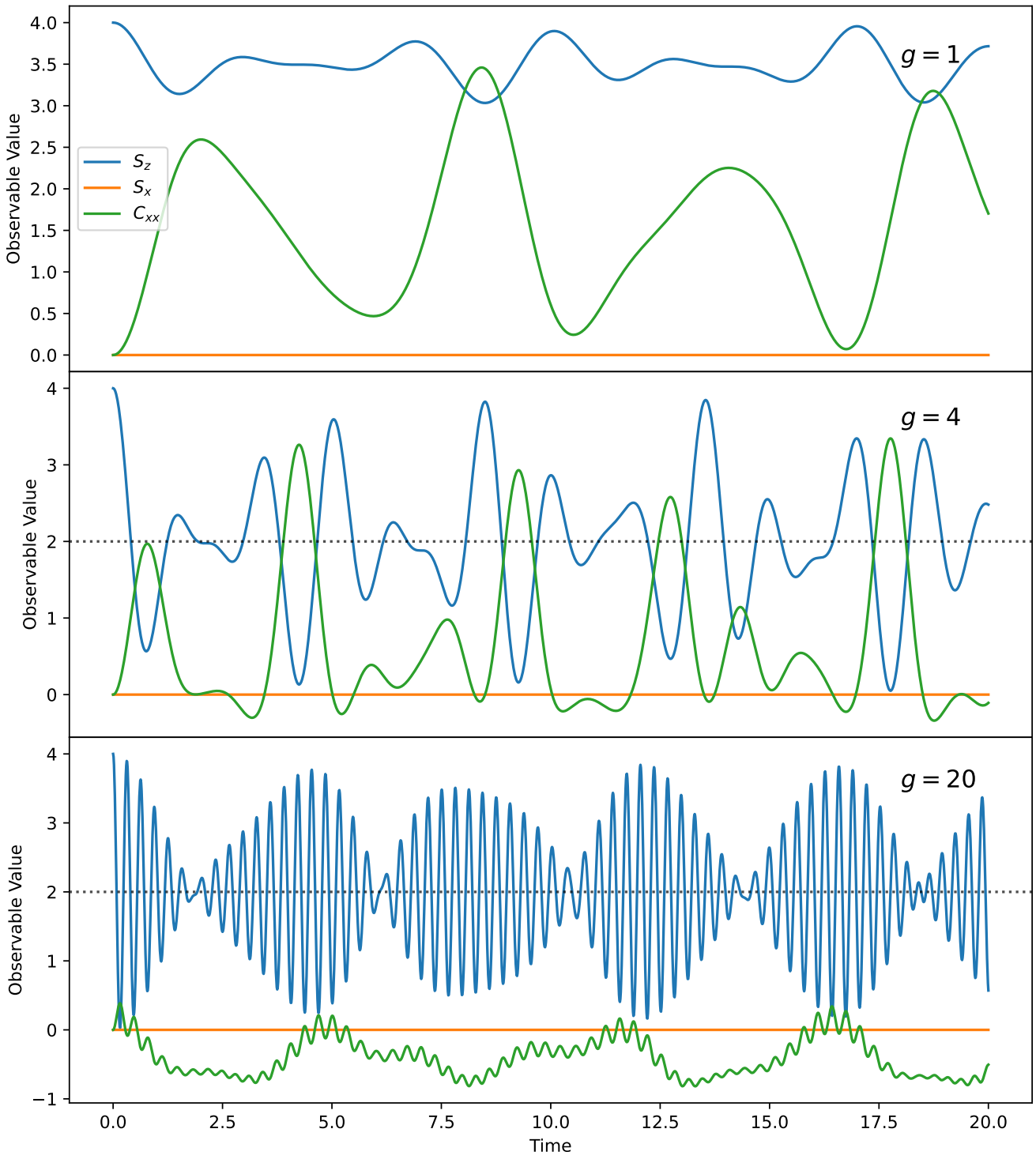

Figure. 7 With $N = 8$ we plot the time evolution of three key observables in the transverse Ising spin model (S_z, S_x, and C_{xx}) after beginning in the $g = 0$ ground state and quenching to $g = 1$, $g = 4$, and $g = 20$ across the panels. We can see that $S_x \simeq 0$ across the duration of all simulations, only discrepant on the order of floating point precision. S_z displays quasi-periodic behaviour, and C_{xx} shows a rough inverse relationship with S_z.